

Figure S1. Constricted migration also increases nuclear blebs in MSCs and DNA damage in A549 cells. DNA damage sites observed tend to be at the center of the nucleus, micronuclei number are slightly increased and BRCA1 mis-localize to cytoplasm. Overexpressed GFP-53BP1 also mis-localize to cytoplasm and does not rescue DNA damage post migration. Migration through larger pores does not perturb nuclear morphology. Related to Figure 1 and Figure 2. (A) Super resolution imaging of a nuclear bleb after constricted migration reveals a dilated meshwork of Lamin-A,C. (B) Cells that have migrated through large 8 μm pores do not exhibit major nuclear damage. (C) Migration of hMSCs through 3 μm pores leads to an increase in nuclear blebs positive nuclei, which is absent of lamin-B (≥ 100 nuclei per conditions, $*p < 0.05$). (D) Migration of A549, human lung carcinoma cell line, through 3 μm pores also leads to an increase in γH2AX foci count (≥ 100 nuclei per conditions, $n \geq 3$ expts, $*p < 0.05$). (E) Nuclear area was segmented to periphery and center by lamin-B integrated intensity. γH2AX foci count reveals that foci tend to be located at the center of the nucleus ($n = 15$ nuclei). (F) DNA damage foci are evident near the pore at bottom and are relatively homogeneous elsewhere ($n = 14$ nuclei). (G) Although higher number of micronuclei were found after 3 μm pore migration, it is relatively rare compared to the pre-dominant nuclear blebs (≥ 3 transwells, $n \geq 3$ expts, $*p < 0.05$). Some of the micronuclei stained for γH2AX , indicative of DNA damage. (H) Specificity of Ku80 antibody was validated by immuno-staining U2OS cells with GFP-Ku80 over-expression. At lower GFP intensity level, Ku80 antibody intensity is statistically the same as the non-transfected cells (dashed line). At higher over-expression level, Ku80 antibody intensity increases proportionally to GFP intensity (≥ 1600 cells). (Inset) Immunoblot of Ku80 and β -actin shows clear bands only at the corresponding molecular weight, again suggesting specificity of the antibodies. (I) Representative images and intensity profiles showing increased BRCA1 mis-localization to the cytoplasm (green shaded) after migration through 3 μm pores at the bottom of the transwell. (J) Live imaging of GFP-53BP1 and H2B-mCherry-overexpressing U2OS cells reveals nuclear rupture—with leakage of GFP/m-Cherry into the cytoplasm. H2B-mCherry signal re-localized rapidly into the nucleus (< 3 hours)[S1]. (K) Over-expression of GFP-53BP1 in U2OS cells does not rescue the migration-induced DNA damage, as shown by the γH2AX foci ratio (≥ 100 cells per conditions, $n \geq 2$ expts).

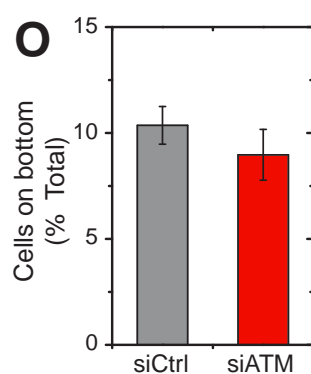
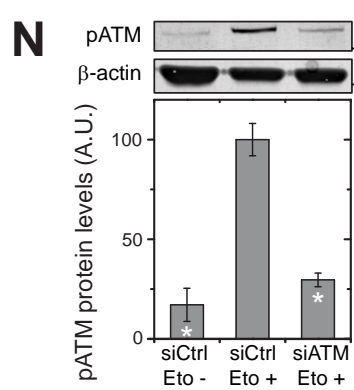
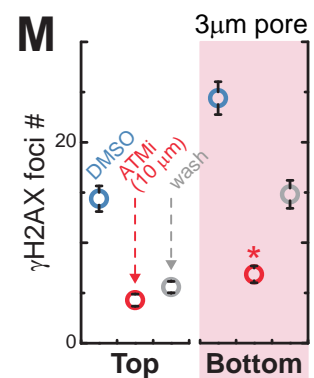
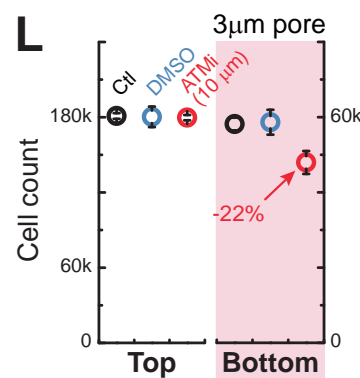
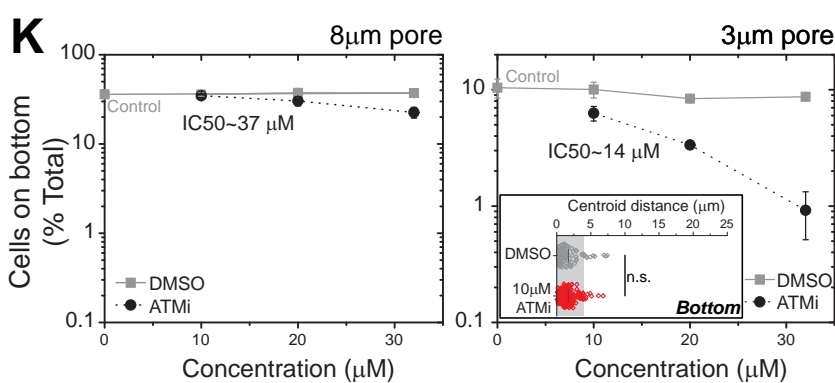
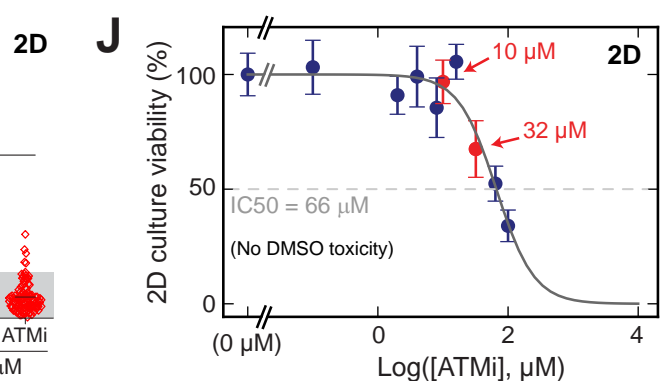
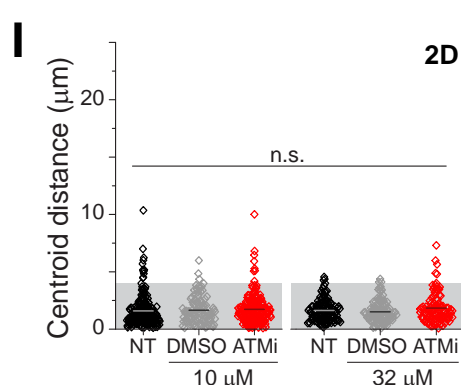
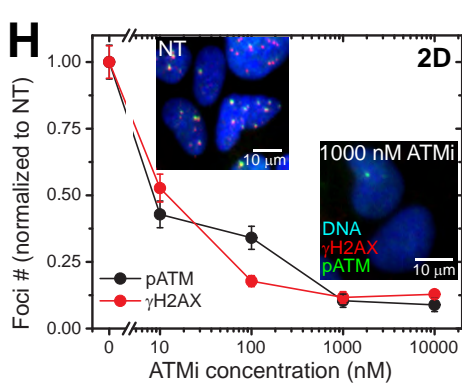
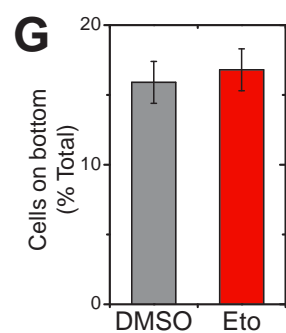
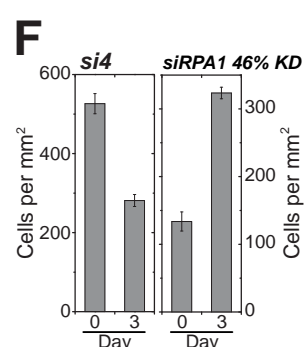
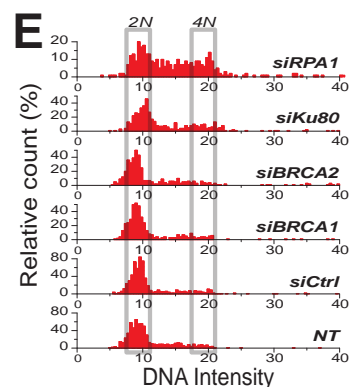
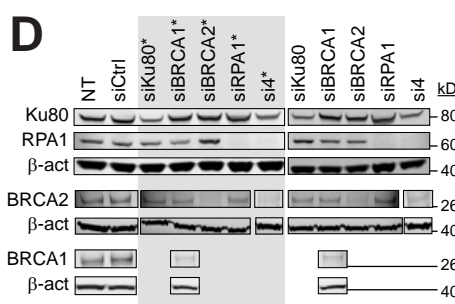
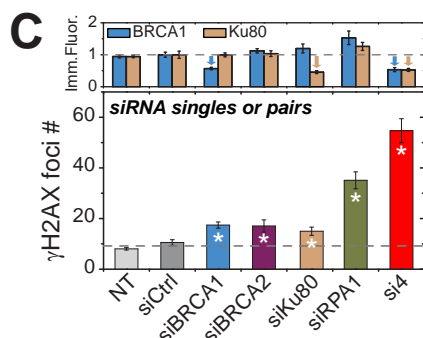
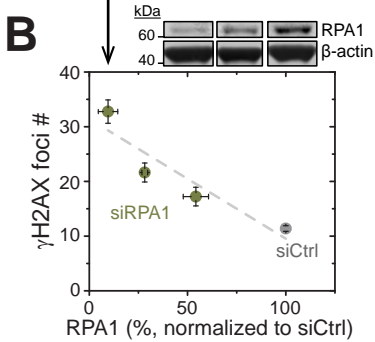
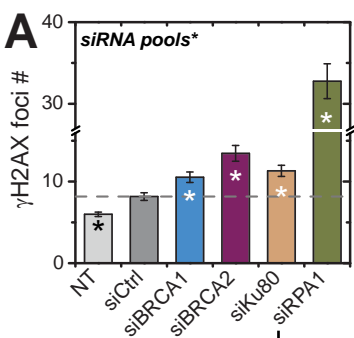
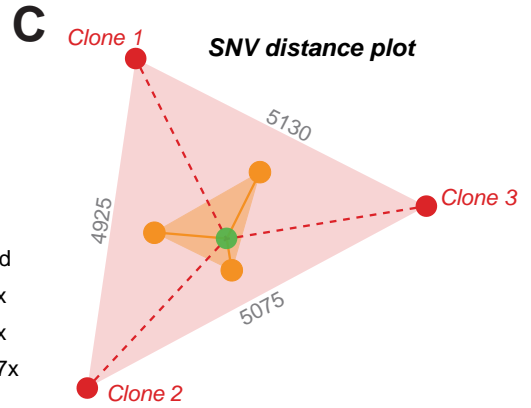
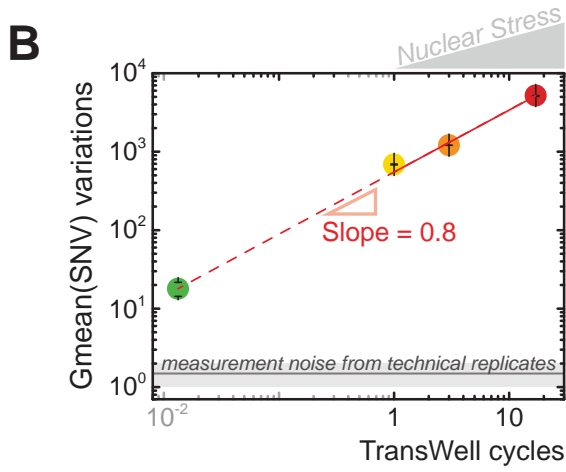
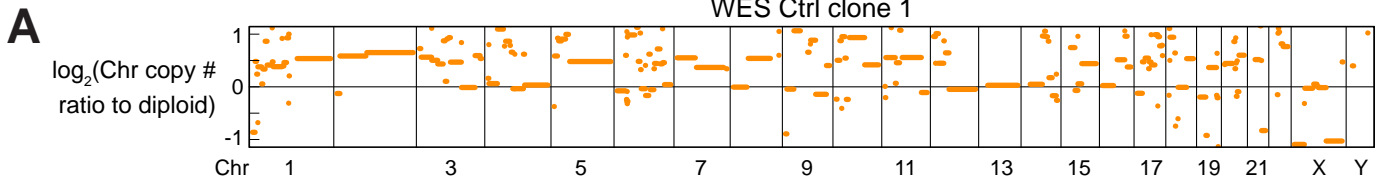


Figure S2. ATMi kills cell on 2D culture at high dosage and after migration with lower dosage. Etoposide-induced DNA damage does not impede migration. Knockdown of some DNA repair factors are titratable and lead to accumulation of DNA damage, increase of DNA content and some cell death. Related to Figure 3. (A) Treating U2OS with single siRNA pool of BRCA1, BRCA2, RPA1 and Ku80 leads to increased γ H2AX foci count. However, the most significant effect was observed in the siRPA1 group (≥ 150 nuclei per conditions, $*p < 0.05$ compared to siCtrl). **(B)** Depletion of siRPA1 is titratable by using less siRNAs, the levels of knockdown are reflected by the γ H2AX foci count, majority of the nuclei have distinctive γ H2AX foci, while minority of nuclei have “global” γ H2AX staining, where the whole nucleoplasmic region is positive for γ H2AX (≥ 150 nuclei per conditions, $n \geq 3$ expts, $*p < 0.05$ compared to siCtrl). **(C)** In order to validate siRNAs specificity, another set of siRNAs with different sequences was purchased from a different source (see Methods). Most of the siRNAs comprise of a single sequence, except for siKu80 that contains a pair of siRNA sequences. Specificity of the knockdown was illustrated by the upper plot, where BRCA1 and Ku80 depletion was only observed in siBRCA1 and siKu80 samples, respectively, in addition to the si4 sample. Indeed, the increase of γ H2AX foci count was also observed with these siRNAs (≥ 150 nuclei per conditions, $n = 2$ expts, $*p < 0.05$ compared to siCtrl). **(D)** Specificity of the DNA repair factors depletion by siRNA treatments was confirmed by immuno-blots (* for the siRNA singles and pairs used in Figure S2C). **(E)** Treating U2OS with single siRNA pools also leads to increased DNA content (≥ 150 nuclei per conditions, $n \geq 3$ expts, $*p < 0.05$ compared to siCtrl, statistical comparison between distributions were done with KS test). **(F)** si4 treatment induces cell death within the 3 days of culture after treatment, but knockdown of RPA1 by 46% allows for cell growth ($n \geq 3$ expts). **(G)** Exposing the cells to 10 μ M Etoposide does not impede the migration, even with the induced DNA damage (Figure 1H, $n = 3$ transwell membranes). **(H, I)** Inhibition efficiency of ATMi was measured by foci counts for γ H2AX and phosphorylated ATM (pATM). Both γ H2AX and pATM foci can be seen in non-treated cells per representative image. Foci counts decreased $\sim 50\%$ at 10 nM and plateau at 0.1 to 1 μ M (≥ 150 nuclei per condition, $n \geq 3$ expts). Comet assay did not show accumulation of DNA damage after ATMi treatment, even at very high drug 32 μ M concentrations (≥ 200 nuclei per group, $n = 3$ expts). **(J)** Colorimetric toxicity assay of ATMi treatment on U2OS 2D culture shows an IC50 of 66 μ M ($n = 3$ expts). **(K)** The percentage of cells that migrated through the transwell in 24 hours is higher for 8 μ m pores than for 3 μ m pores, and is reduced only for very high doses of ATMi (10, 20 and 32 μ M), with 50% fewer cells (IC50) of 37 and 14 μ M for 8 μ m and 3 μ m pores, respectively. DMSO solvent control does not affect the migration ratios (≥ 3 transwell each condition, $n \geq 3$ expts). The inset shows 10 μ M ATMi during migration also does not cause more comet-detected DNA damage when compared to the corresponding DMSO group (≥ 200 nuclei each condition, $n \geq 3$ expts). **(L, M)** Inhibition with ATMi (10 μ M) of ATM kinase which phosphorylates H2AX (to make γ H2AX) during the 24 hrs of constricted migration decreases cell numbers on the Bottom but not the Top. The result is consistent with past evidence of migration-dependent cell death. For both Top and Bottom, ATMi strongly decreases γ H2AX, but more foci on Bottom are resistant (≥ 45 nuclei per condition, $n \geq 3$ expts, $*p < 0.05$). **(N)** siATM treatment leads to a decrease of pATM in samples exposed to 10 μ M etoposide ($n = 3$ western blots, $*p < 0.05$ compared to siCtrl treated with etoposide). **(O)** siATM does not inhibit migration ($n = 3$ transwell membranes).



D

	Control Clone1	Control Clone2	Control Clone3	Control Clone4	Control Clone5	Control Clone6	TW3 Clone1	TW3 Clone2	TW3 Clone3	TW17 Clone1	TW17 Clone2	TW17 Clone3
Control-Clone1	0	36	0	32	13	2	1043	394	866	2455	2508	2626
Control-Clone2	36	0	36	32	13	4	1079	430	902	2491	2544	2662
Control-Clone3	0	36	0	32	13	2	1043	394	866	2455	2508	2626
Control-Clone4	32	32	32	0	21	34	1075	426	898	2455	2529	2660
Control-Clone5	13	13	13	21	0	15	1056	407	879	2476	2508	2641
Control-Clone6	2	4	2	34	15	0	1045	398	868	2489	2523	2626
TW3-Clone1	1043	1079	1043	1075	1056	1045	0	1433	1907	3494	3547	3665
TW3-Clone2	394	430	394	426	407	398	1433	0	1258	2845	2592	3016
TW3-Clone3	866	902	866	898	879	868	1907	1258	0	3319	1746	3462
*TW17-Clone1	2455	2491	2455	2455	2476	2489	3494	2845	3319	0	4925	5075
*TW17-Clone2	2508	2544	2508	2529	2508	2523	3547	2592	1746	4925	0	5130
*TW17-Clone3	2626	2662	2626	2660	2641	2626	3665	3016	3462	5075	5130	0

E Expt 1

	Clone 1	Clone 2	Clone 3	Clone 4	Clone 5	Clone 6
Pre-migration clone (Gain)	0	0	24	38	53	72
Pre-migration clone (Loss)	0	0	1	0	1	2
Pre-migration clone (Total)	0	0	25	38	54	74
Clone 1	0	0	25	38	55	74
Clone 2	0	0	25	38	55	74
Clone 3	25	25	0	63	80	75
Clone 4	38	38	63	0	93	154
Clone 5	55	55	80	93	0	128
Clone 6	74	74	75	154	128	0

F Expt 2

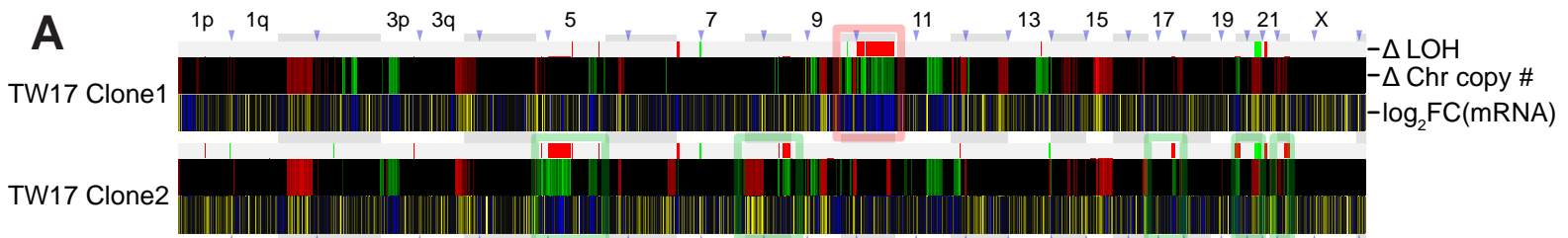
	TW3 clone 1	TW3 clone 2	TW3 clone 3
Ctrl clone 1 (Gain)	15	27	15
Ctrl clone 1 (Loss)	4	0	5
Ctrl clone 1 (Total)	19	27	20
TW3 clone 1	0	49	49
TW3 clone 2	49	0	58
TW3 clone 3	49	58	0

G Expt 3

	3 μm clone 1	3 μm clone 2	3 μm clone 3	3 μm clone 4
Ctrl clone 1 (Gain)	0	6	10	28
Ctrl clone 1 (Loss)	0	0	0	0
Ctrl clone 1 (Total)	0	6	10	28
3 μm clone 1	0	7	21	30
3 μm clone 2	7	0	10	37
3 μm clone 3	21	10	0	35
3 μm clone 4	30	37	35	0

	8 μm clone 1	8 μm clone 2	8 μm clone 3	8 μm clone 4	8 μm clone 5	8 μm clone 6
Ctrl clone 1 (Gain)	0	0	0	0	8	17
Ctrl clone 1 (Loss)	0	0	0	0	0	0
Ctrl clone 1 (Total)	0	0	0	0	8	17
8 μm clone 1	0	0	0	0	8	20
8 μm clone 2	0	0	0	0	9	17
8 μm clone 3	0	0	0	0	9	19
8 μm clone 4	0	0	0	0	10	17
8 μm clone 5	8	9	9	10	0	27
8 μm clone 6	20	17	19	17	27	0

Figure S3. Chromosome copy number derived from whole exome sequencing (WES) data agrees with data of aCGH. Number of SNVs increase with migration, increasing the heterogeneity of the cell population. Variations in Δ LOH is smallest for clones migrated through 8 μ m transwells. Related to Figure 4 and Figure 5. (A) Chromosome copy number derived from whole exome sequencing (WES) data of control clone 1 agrees with the aCGH data in Figure 4C. Chromosome copy number from control clone 1 WES data was acquired by using CNVkit software package, compared against the computed “flat” diploid reference[S2], then the data were shifted up (by $\log_2(0.3)$) such that the diploid regions of WES and aCGH agree with each other, i.e. chromosome 4q, 12q and 13. CNVkit is best for comparisons of two samples, where data shifting is not required, as done in Figure S4. (B,C) Considering the data from Figure 5, instead of comparing to Ctrl clone 1, the three clones of each group are compared to each other. As the cells migrate, SNVs between clones increase. Measurement noise is derived from technical controls from multiple arrays ($n \geq 3$ clones per condition). (D) SNV heatmap showing pairwise comparisons of the different SNPa samples. Numbers in the heatmap indicate number of probes detected within the SNV pair comparison. Bulk samples and control clones have relatively low SNVs, indicative of a homogeneous population. Migrations through the 3 μ m transwells increase number of SNVs. (E,F,G) SNV confirmed changes in LOH’s (in Mb, see text or methods) of TW3 clones from experiment 1 (Figure 4E-H), 2 (Figure 5A-D) and 3 are listed as LOH gain, loss and total (gain+loss). Pairwise comparison of the clones are listed below row 3 of each heatmap. Most of the LOH gains are confirmed by SNV calls, but not LOH losses. LOH variations are lowest after 8 μ m migration.



ΔChr copy # (■ SNP/ ◆ WES) ● ΔLOH △ log₂FC(mRNA) ▼ log₂FC(mRNA) Top 10%

Δ LOH Δ Chr copy # log₂FC(mRNA)

-1 0 1 -2 0 2 -2 0 2

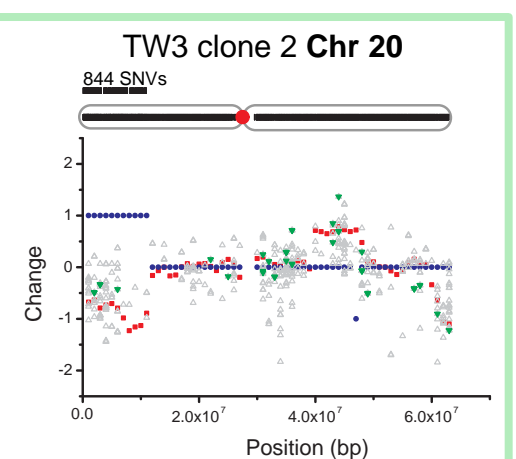
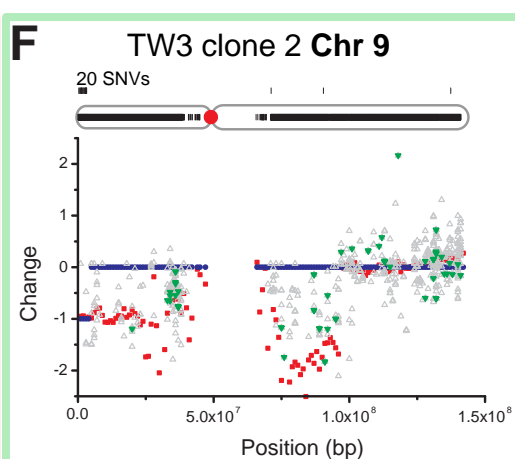
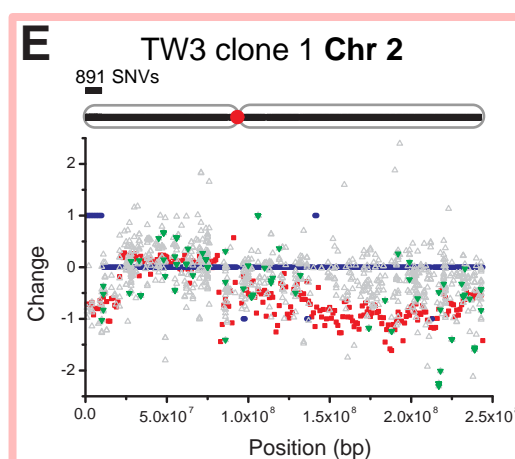
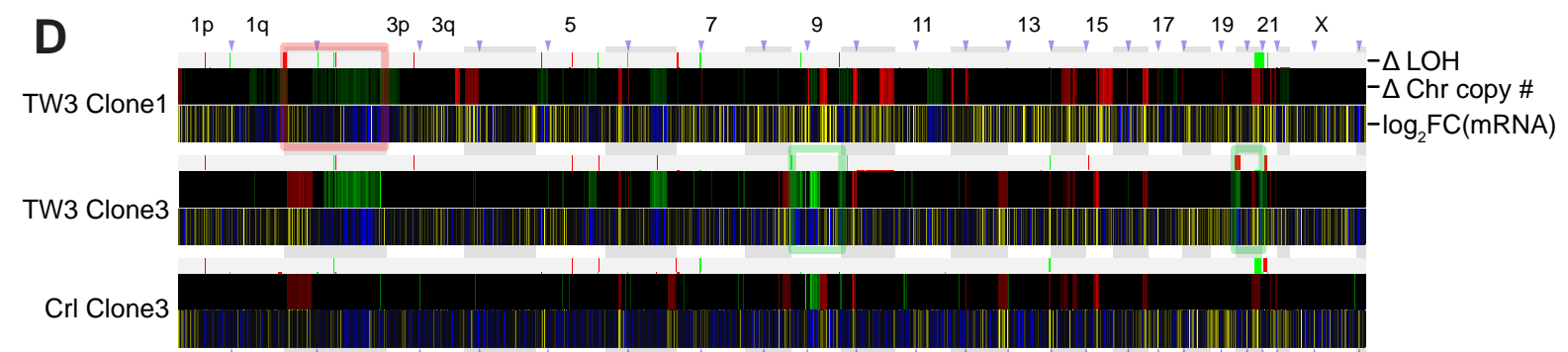
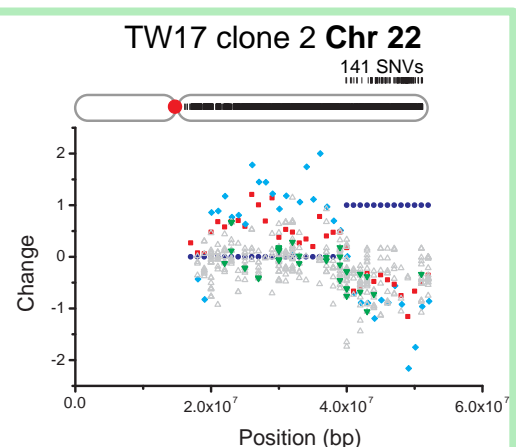
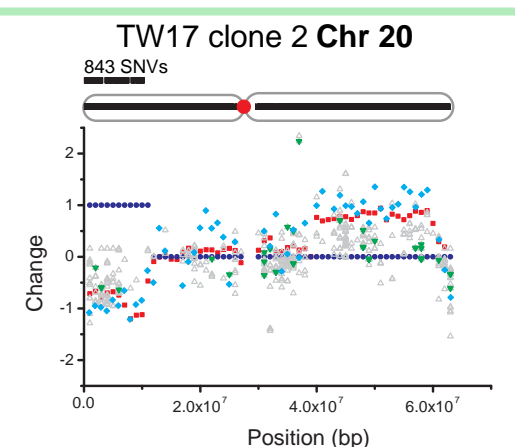
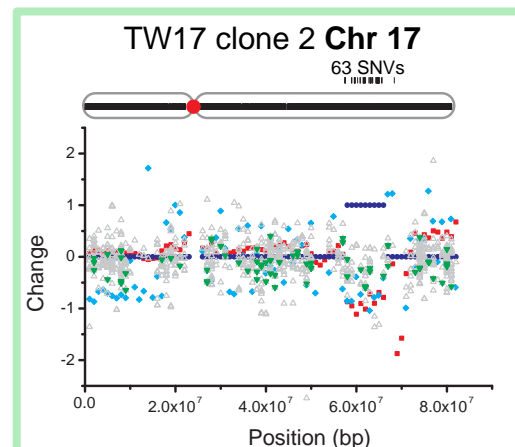
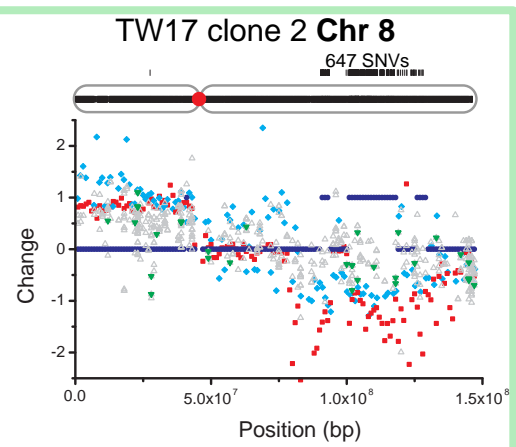
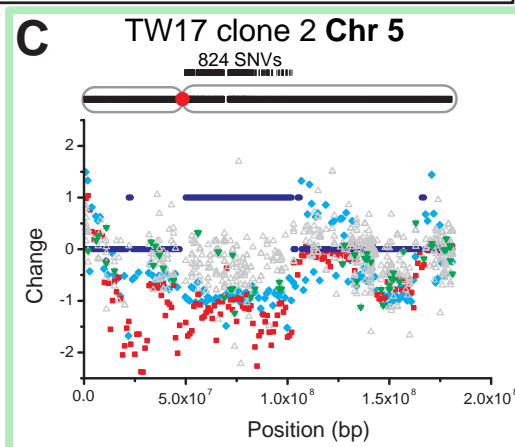
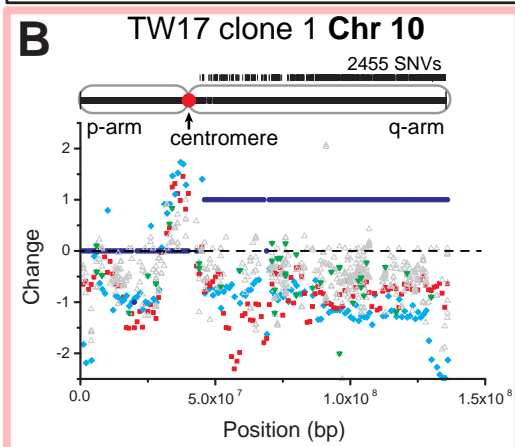


Figure S4. mRNA, Δ CN, Δ LOH and SNVs data are consistent with each other, showing partial loss and gain of the chromosomes. Related to Figure 5. (A,D) Change in LOH (Δ LOH), change in chromosome copy number (Δ Chr copy #) and log₂ of mRNA fold change (log₂FC(mRNA)) heatmaps from the study involved in Figure 5. Although the samples here are subtracted by the data of Control clone 1, differences between samples are still observed and also increase with number of constricted migration, as shown in Figure 5 when samples were subtracted by pre-migration sample. Consistent patterns can be observed between Δ Chr copy # and log₂FC(mRNA), when a region gain chromosome copy number (red), it is often accompanied by an increase in mRNA levels (yellow), and vice versa. Compliment of Figure 5G. **(B,C,E,F)** Various chromosomal plots from the heatmaps in Figure S4A, providing a zoomed in plot of a given chromosome for Δ Chr copy # from SNP array (SNPa) and whole exome sequencing (WES), Δ LOH, SNVs and mRNA fold change. Black ticks on top of each plot indicate the SNPa probes location for a given chromosome, with reference to the centromere (red circle). SNVs are indicated as an upward shift of the ticks. The more reliable highly abundant transcripts (top 10% expressing mRNAs, green) also follow the Δ Chr copy # pattern.

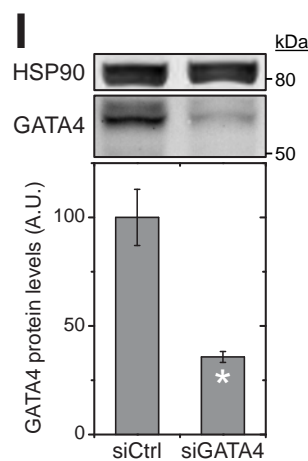
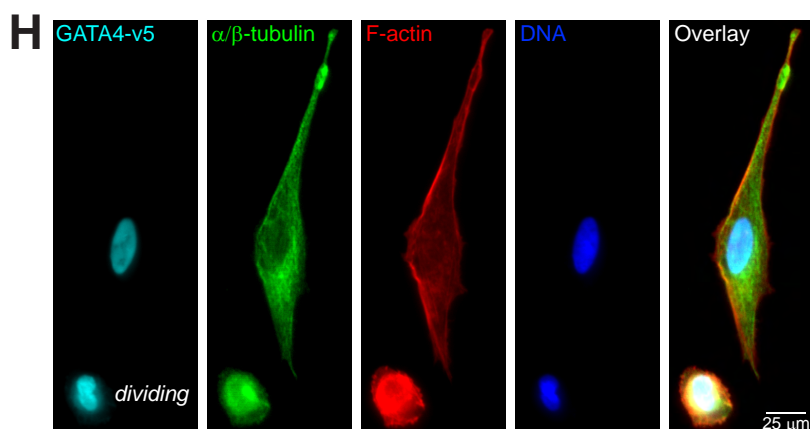
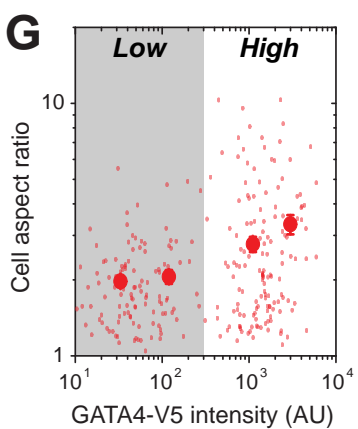
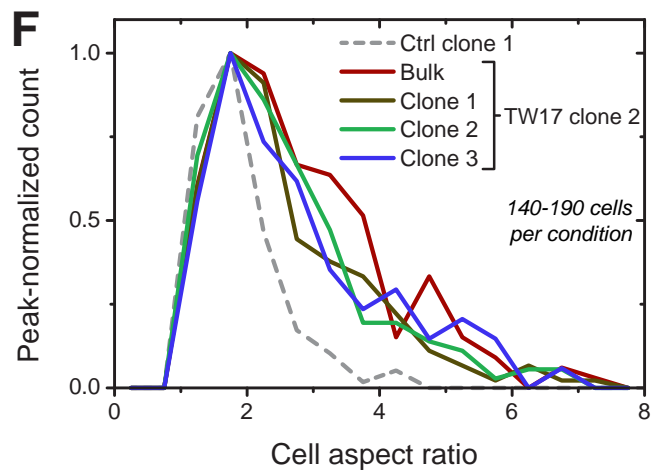
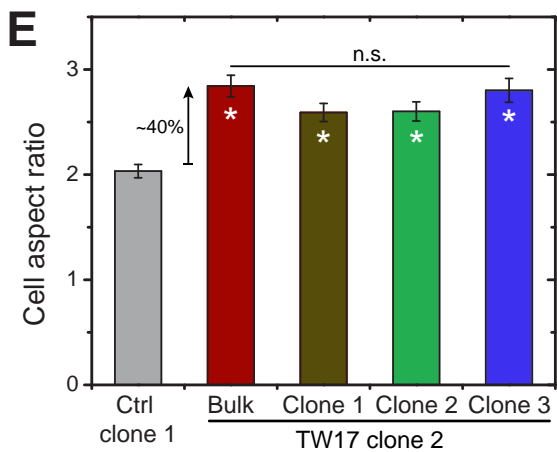
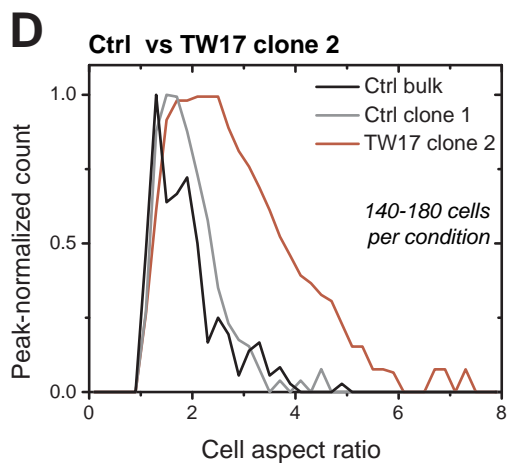
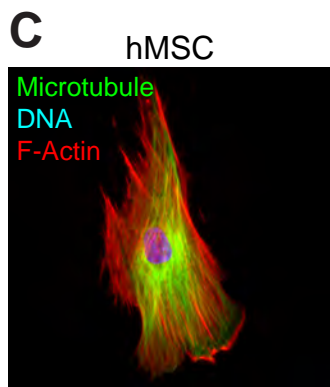
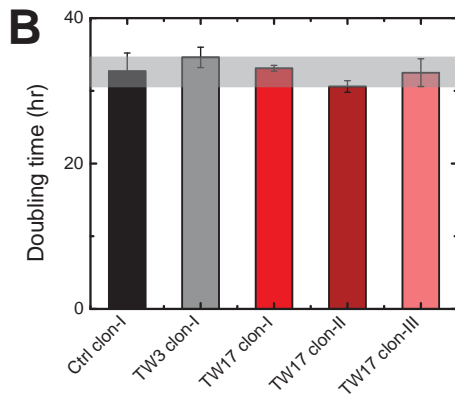
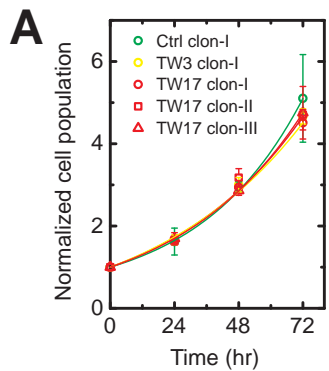


Figure S5. Multiple constricted migration does not alter proliferation rate, but one of the migrated clone has altered cell morphology. The elongated morphology is driven by tubulin organization and GATA4, which can be depleted by siGATA4 treatment. Related to Figure 6. (A,B) Proliferation rate and doubling time stay relatively constant between the non-migrated and migrated clones. **(C)** hMSC showing alignment of microtubule along the length of the cell, giving it an elongated cell morphology. **(D)** Cell aspect ratio distribution of Ctrl bulk, Ctrl clone 1 and TW17 clone 2, showing the shift to an elongated cell morphology for TW17 clone 2 (≥ 140 cells per condition, $n \geq 3$ expts, $*p < 0.05$). **(E,F)** Single cell clones were isolated from TW17 clone 2 and their cell morphology were quantified from F-actin staining by phalloidin. Both averaged aspect ratio and distribution of the clones are similar to the bulk TW17 clone 2 ($*p < 0.05$ compared to Ctrl clone 1). **(G)** Cell aspect ratio scatter plot of cells expressing GATA4-v5, showing an increase in aspect ratio with higher GATA4-v5 expression. **(H)** Highly spindle U2OS with the overexpression of GATA4-v5 has microtubules along the length of the cell, resemblance of hMSC in (C). **(I)** siGATA4 treatment on TW17 clone 2 cells leads to a decrease in GATA4 protein levels ($n = 3$ western blots, $*p < 0.05$ compared to siCtrl).

Table S1. Clonality of U2OS cultures as measured by comparative genome hybridization arrays, aCGH. Related to Figure 4 and 5, with additional information in Table S6.

Culture	% clonality
Control bulk	87.2%
Control clone 1	95.2%
TW3 clone 1	95.5%
TW3 clone 2	100%
TW3 clone 3	98.9%
TW17 clone 1	100%
TW17 clone 2	98.7%
TW17 clone 3	100%

Table S2. Chromosome number estimates were derived from aCGH data for Control bulk and clone 1 sample in Figure 4B-C. Chromosome total length of each chromosome was calculated by adding the chromosome copy number calls of the corresponding chromosome. Chromosome number was estimated by dividing the chromosome total length by the 1 Mb windows of each chromosome, hence it is the average chromosome copy number call.

<u>Control bulk</u>	<u>Chr</u>	<u>Chr number estimate</u>	<u>Chr total length (Mb)</u>
	1	2.98	682.29
	2	3.21	775.70
	3	2.73	534.71
	4	2.51	474.62
	5	3.05	542.07
	6	2.70	455.91
	7	2.61	411.85
	8	3.50	507.17
	9	2.77	340.80
	10	3.24	433.66
	11	2.83	375.79
	12	2.75	362.55
	13	2.06	199.71
	14	2.87	255.64
	15	2.89	240.01
	16	2.88	233.31
	17	3.07	245.94
	18	2.65	203.97
	19	2.51	145.45
	20	3.13	191.01
	21	2.83	102.04
	22	4.29	154.52
	X	1.57	237.75
	TOTAL	65.62	8106.47

<u>Control clone 1</u>	<u>Chr</u>	<u>Chr number estimate</u>	<u>Chr total length (Mb)</u>
	1	2.93	669.83
	2	3.05	736.97
	3	2.75	538.69
	4	2.56	483.53
	5	3.07	546.90
	6	2.61	441.24
	7	2.69	425.22
	8	3.21	465.58
	9	2.88	354.05
	10	3.24	433.80
	11	2.98	395.74
	12	2.61	344.28
	13	2.13	206.20
	14	2.77	246.57
	15	2.72	225.35
	16	2.83	229.01
	17	3.09	247.32
	18	2.66	204.90
	19	2.49	144.16
	20	2.98	181.59
	21	2.69	96.84
	22	4.30	154.68
	X	1.55	233.84
	TOTAL	64.75	8006.27

Table S4. Counts taken from the chromosome copy number change against $\log_2(\text{RNA ratio})$ plots shown in Figure 5G. **Only the data points above the 0.5 threshold**, for both changes, were taken into consideration. Relative percentage population of each sample for each quadrants of table S2A. For overall positive correlation, we combined the data as cluster 2 & 3 (C2, C4) versus cluster 1 & 4 (C1, C4), and calculated $p = 3.15 \times 10^{-9}$. Probability of the positive correlation between the chromosome copy number change against $\log_2(\text{RNA ratio})$, per counts. Probability of each cluster was calculated by $0.5^{(\text{Count})}$ for the counts listed in upper table. The positive correlation p-value was calculated by $(pC3/pC1) * (pC2/pC4)$. Cluster 1, 2, 3 and 4 represent top left, top right, bottom left and bottom right quadrants of the plot.

Counts	Ctrl Clone 1	Ctrl Clone3	TW3 Clone1	TW3 Clone3	TW17 Clone1	TW17 Clone2
Cluster1	26	20	71	64	60	101
Cluster2	161	178	347	203	384	340
Cluster3	108	164	302	294	246	220
Cluster4	133	135	131	87	226	94
TOTAL	428	497	851	648	916	755

Percentage population

Cluster1	6.1%	4.0%	8.3%	9.9%	6.6%	13.4%
Cluster2	37.6%	35.8%	40.8%	31.3%	41.9%	45.0%
Cluster3	25.2%	33.0%	35.5%	45.4%	26.9%	29.1%
Cluster4	31.1%	27.2%	15.4%	13.4%	24.7%	12.5%

Probability

pCluster1	1.5E-08	9.5E-07	4.2E-22	5.4E-20	8.7E-19	3.9E-31
pCluster2	3.4E-49	2.6E-54	3.5E-105	7.8E-62	2.5E-116	4.5E-103
pCluster3	3.1E-33	4.3E-50	1.2E-91	3.1E-89	8.8E-75	5.9E-67
pCluster4	9.2E-41	2.3E-41	3.7E-40	6.5E-27	9.3E-69	5.0E-29
Positive correlation p-value	7.7E-34	5.1E-57	2.8E-135	7.0E-105	2.8E-104	1.3E-110

Table S5. Counts taken from the chromosome copy number change against $\log_2(\text{RNA ratio})$ plots shown in Figure 5G. **All data points were taken into consideration.** Relative percentage population of each sample for each quadrants of table S2A. For overall positive correlation, we combined the data as cluster 2 & 3 (C2, C4) versus cluster 1 & 4 (C1, C4), and calculated $p=0.008$. Probability of the positive correlation between the chromosome copy number change against $\log_2(\text{RNA ratio})$, per counts. Probability of each cluster was calculated by $0.5^{(\text{Count})}$ for the counts listed in upper table. The positive correlation p-value was calculated by $(pC3/pC1)*(pC2/pC4)$. Cluster 1, 2, 3 and 4 represent top left, top right, bottom left and bottom right quadrants of the plot.

Counts	Ctrl Clone 1	Ctrl Clone3	TW3 Clone1	TW3 Clone3	TW17 Clone1	TW17 Clone2
Cluster1	96	125	174	275	162	388
Cluster2	818	522	1007	684	863	873
Cluster3	311	735	503	700	410	493
Cluster4	1149	992	690	715	939	620
TOTAL	2374	2374	2374	2374	2374	2374


Percentage population

Cluster1	4.0%	5.3%	7.3%	11.6%	6.8%	16.3%
Cluster2	34.5%	22.0%	42.4%	28.8%	36.4%	36.8%
Cluster3	13.1%	31.0%	21.2%	29.5%	17.3%	20.8%
Cluster4	48.4%	41.8%	29.1%	30.1%	39.6%	26.1%

Probability

pCluster1	1.3E-29	2.4E-38	4.2E-53	1.6E-83	1.7E-49	1.6E-117
pCluster2	5.7E-247	7.3E-158	7.3E-304	1.2E-206	1.6E-260	1.6E-263
pCluster3	2.4E-94	5.5E-222	3.8E-152	1.9E-211	3.8E-124	3.9E-149
pCluster4	9.3E-302	2.4E-299	1.9E-208	5.8E-216	2.2E-283	2.3E-187
Positive correlation p-value	1.2E-10	7.2E-43	3.4E-195	2.5E-119	1.7E-52	1.7E-108

Table S6. Results from array-CGH (Comparative Genome Hybridization) for control clone 1 of Figure 4C.

	www.dgenetics.com
510 Chormany Drive • #254-255 • Madison, Wisconsin 53719 • 608-441-8160	
CLG Microarray Test Results	
Cell Line ID: U2OS/Control-Clone1 p8 Lab #: CLG-21818 Date received: 11/6/15 Date Reported: 11/20/15	
Contact Person: Jerome Irianto	PI: D. Discher Institute: University of Pennsylvania
Test Code: aCGH 150 Email: iriantoj@seas.upenn.edu	PO #: 3473145
Mailing Address: 129 Towne Building, 220 S. 33 rd St., Philadelphia, PA 19104	
<hr/>	
Sample Type: Human Epithelial Frozen Culture dsDNA Concentration: 218ng/μl Total dsDNA: 3.2 μg	
Sex: Female 260/280 (1.7-1.9): 1.8 260/230 (≥1.90): 2.2 Array Type: Agilent 180K Standard aCGH +SNP	
Array ID Number: 252983030028_1_1 Reference DNA: Agilent Euro Female	
<hr/>	
Quality Control	
A sufficient amount of high quality genomic DNA, as determined by UV spec. (NanoVue), fluorometer (Qubit) and Agarose Gel analysis, was extracted from cell line U2OS/Control-Clone1 p8 and passed our internal quality standards for aCGH labeling.	
aCGH Probes (PASS/FAIL): Pass	
SNP Probes (PASS/FAIL): Pass	
Experimental Deviations: None	
Results:	
Clonal Fraction: 95.17%	
See attached sheets for Tabular and Graphical presentation of microarray results.	
Variants are considered provisional until confirmed by another technique. For further confirmation of a particular variant, CLG recommends using Karyotyping (variants >5Mb), FISH (variants >200Kb).	

Supplemental References

- S1. Irianto, J., Pfeifer, C.R., Bennett, R.R., Xia, Y., Ivanovska, I.L., Liu, A.J., Greenberg, R.A., and Discher, D.E. (2016). Nuclear constriction segregates mobile nuclear proteins away from chromatin. *Mol. Biol. Cell.* DOI: 10.1091/mbc.E16-06-0428
- S2. Talevich, E., Shain, A.H., Botton, T., and Bastian, B.C. (2016). CNVkit: Genome-Wide Copy Number Detection and Visualization from Targeted DNA Sequencing. *PLoS Comput. Biol.* 12, e1004873.